LDV measurements in turbulent gaseous mixing induced by the Richtmyer-Meshkov instability: statistical convergence issues and turbulence quantification

Ghazi Bouzgarrou
Yannick Bury*
Stéphane Jamme
Laurent Joly

Université de Toulouse
Institut Supérieur de l'Aéronautique et de l'Espace (ISAE)
10 avenue Edouard Belin, 31400 Toulouse
France
Email: yannick.bury@isae.fr

Jean-François Haas
CEA, DAM, DIF
F-91297, Arpajon
France

ABSTRACT

A statistical characterization of the turbulent flow produced in a vertical shock tube dedicated to the study of the Richtmyer-Meshkov instability (RMI) is carried out using Laser Doppler Velocimetry (LDV), time-resolved Schlieren images and pressure histories. The time evolution of the phase-averaged velocity field and the fluctuating velocity levels produced behind the shock wave are first investigated for different configurations of a pure air, homogeneous medium. This allows us to determine the background turbulence of the experimental apparatus. Second, the RMI-induced turbulent Air/SF_6 mixing zone (TMZ) is studied both in its early stage of development and after its interaction with a reflected shock wave (reshock phenomenon). Here the gaseous interface is initially produced by a thin nitrocellulosic membrane trapped between two grids. One of the most consistent issue regarding such a process is the generation of a large number of fragments when the incident shock wave crosses the interface. These fragments are likely to corrupt the optical measurements and to interact with the flow. This work seeks to clarify the influence of these fragments on the statistical determination of the velocity field. In particular it is shown that statistical convergence cannot be achieved when the fragments are crossing the LDV measurement volume, even if a significant number of identical experiments are superimposed. Some specific locations for the

*Address all correspondence to this author.

LDV measurements are however identified to be more favourable than others in the Air/SF_6 mixing configuration. This finally allows us to quantify the surplus of turbulence induced by the reshock phenomenon.

1 Introduction

The Richtmyer-Meshkov instability (RMI) occurs when a shock wave impulsively accelerates a perturbed interface between two gases of different densities. The interaction of the shock wave with the perturbed interface promotes the production of vorticity through baroclinic effects, potentially leading to the development of a turbulent mixing zone (TMZ). The RMI is observed in several engineering applications or natural phenomena, *e.g.* inertial confinement fusion, supersonic combustion or supernova explosion. Since the pioneering works of Taylor [1], Richtmyer [2] and Meshkov [3], the linear and non-linear stages of the RMI-induced perturbations of the interface have been and are still widely studied [4], either theoretically, numerically and experimentally for a wide variety of well-characterized initial conditions.

In contrast, the consecutive turbulent stages corresponding first to the TMZ development and second to its interaction with a reshock are still poorly documented, despite their practical interest. In order to analyze the late turbulent phase of the mixing, a three-dimensional random perturbation is generally imposed to the initial interface in order to promote the rapid transition to a turbulent state. Most of the corresponding experiments [3, 5–9] have been conducted in shock tubes where the two gases are initially separated by a thin nitrocellulosic membrane. Aternative solutions have also been proposed to obviate the need of a membrane [10, 11]. One should however mention the technical complexity of such membraneless experiences and the difficulty in controlling both the shape of the initial perturbation and diffusive effects. These solutions will not be further discussed in this paper. Considering the membrane-separated interface experiments, one of the main resulting drawbacks is the generation of fragments in the flow consecutive to the breakup of the membrane by the incident shock wave. Their influence on the growth rate of the mixing zone has been investigated by Erez *et al.* [12] who found that this effect is only noticeable during the initial stages of the TMZ development (before the reshock), when the amplitude of the perturbations is small, and is negligible when the amplitude of the perturbations gets larger (after the reshock). However, even if the temporal growth rate of the TMZ is of prime interest for the study of the late turbulent phase of the RMI-induced mixing, a thorough understanding of the mechanisms driving the spatio-temporal evolution of the TMZ still suffers a lack of comprehensive analysis. This can be partly addressed by quantifying the turbulence levels experienced during the RMI-induced mixing phase. This can be achieved using Laser Doppler Velocimetry (LDV), through the optical measurement of the instantaneous velocity at specific locations inside the flow. Velocity statistics are then obtained by averaging over a sufficient number of identical experiments. To the authors' knowledge, the only published work following this approach can be found in Poggi *et al.* [8]. This lack of data is due to the difficulty in getting converged statistics because of the presence of membrane fragments inside the flow that drastically reduce the temporal acquisition rate, hereafter denoted data rate, of the velocity measurements when they are crossing the LDV probe volume. One of the objectives of the present paper is to address this issue by applying the above-mentioned approach in a light/heavy gas configuration with an Atwood number of 0.67, which corresponds to the crossing of the shock wave from air to sulfur hexafluoride (SF_6). In particular this requires to estimate the number of identical experiments necessary to ensure the convergence of the velocity statistics. This paper also

serves the identification of the most favourable locations for LDV measurements and the quantification of the influence of the fragments on the mixing process, through, *e.g.*, a potential surplus of turbulence production. More generally it aims at shedding light on the mixing process before and after the reshock phenomenon.

This paper is organized as follows. Section 2 is dedicated to the description of the experimental test-rig. Section 3 provides a characterization of the 'background turbulence' of the shock tube by performing LDV measurements without any membrane fragments and without mixing (pure air configuration). Then we estimate the influence of the membrane fragments on the statistical convergence and on the turbulence levels measured in the flow, first in pure air configuration (section 4), second in Air/SF_6 mixing configuration (section 5). Finally some insights are provided about the surplus of turbulent fluctuations induced in the mixing zone by the reshock phenomenon.

2 Experimental setup and diagnostics

2.1 Description of the experimental setup

The experimental setup, sketched in Fig. 1, consists in a 5m long, 130mm square cross section vertical shock tube. For studies involving RMI and the resulting turbulent mixing, a shock wave (Mach number 1.2) travels upwards and crosses an air/SF_6 interface, which sets the Atwood number at 0.67. The two gases are initially separated by a thin nitrocellulosic membrane (0.5 μm thick) trapped between two square-meshed grids. The lower grid (mesh-spacing: 1mm, wire diameter: 70 μm, transparency: 87%) ensures the mechanical resistance of the membrane under hydrostatic pressure of the heavy gas. The upper grid, of wire diameter 230 μm and of transparency 76%, imposes a three-dimensional initial perturbation of wavelength equal to 1.8 mm, corresponding to its mesh-spacing. An illustration of the pattern of the initial perturbation is provided in Fig. 2. In their study about the turbulent gaseous mixture induced by RMI, Poggi *et al.* [8] have shown that such a perturbation imposes a fully developed turbulence in a short time compared to the arrival time of the mixing zone at measurement locations comparable to the ones addressed in the present study.

A schematic of the experimental setup is shown in Fig. 1. All the experiments presented in this work are conducted with a test section length $L = 250$ mm. The Mach 1.2 incident shock wave is generated by impacting a Mylar diaphragm, initially separating the driven (Low Pressure, LP) and the driver (High Pressure, HP) sections of the shock tube, using a cross-shaped sharp edges cutting device. The pressure in the driver section is controlled via a Keller pressure transmitter with an accuracy of 0.1% of the full range (0-3bars relative to the ambient pressure). The electro pneumatic device driving the cutting device is a Joucomatic Uniclair C25-AS-50 electrovalve. The pressure applied in the electro-pneumatic impacting device is controlled via a Keller pressure transmitter (0-5bars relative to the ambient pressure).

2.2 Diagnostics

Pressure histories of the flow in the shock tube are recorded using five flush-mounted piezoelectric pressure transducers. The acquisition frequency is fixed to 500 kHz which corresponds to the cut-off frequency of the pressure transducers and their associated charge amplifiers. For each experiment, the incident Mach number is determined via the detection of the shock wave by PPT1 and PPT2 pressure transducers located at $X = -315$ mm and $X = -115$ mm, relative to the interface position,

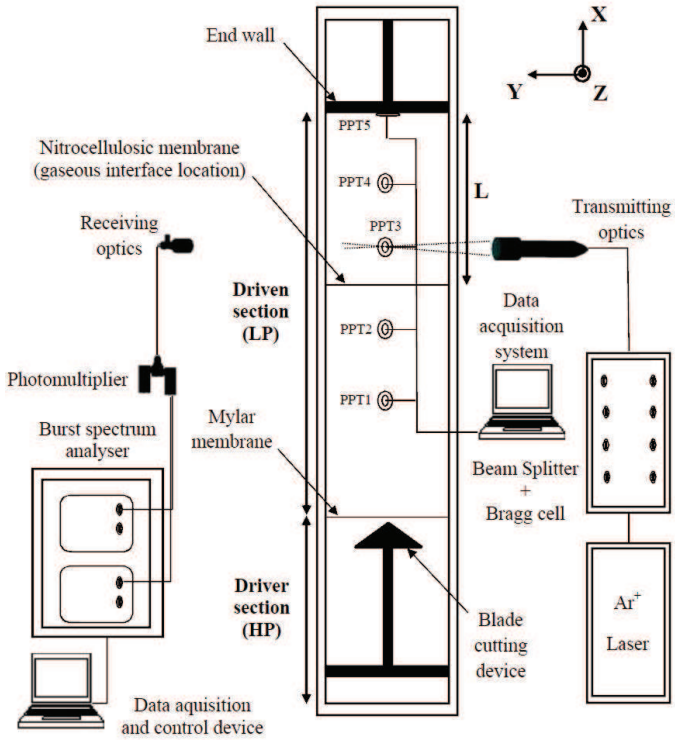

Fig. 1. Description of the experimental apparatus.

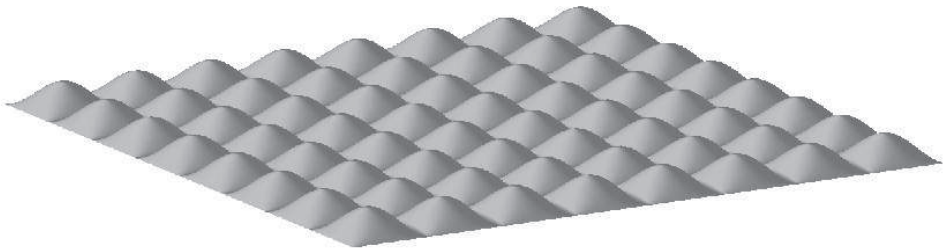

Fig. 2. Illustration of the pattern of the initial perturbation.

respectively (Fig. 1). In the test section, three additional pressure transducers PPT3, PPT4 and PPT5 are flush-mounted at $X = 43$, 213 and 250 mm above the interface respectively.

For a given configuration, the set of instantaneous LDV measurements obtained from the corresponding set of runs are synchronized on the time of detection t_0 of the shock wave on the LDV signals (in other words, the instant of passage of the shock wave in the LDV probe volume). An ensemble averaging, hereafter denoted phase-averaging, is then applied and phase-averaged mean ($\overline{U}$) and r.m.s. fluctuating ($\sqrt{\overline{u'^2}}$) $X-$velocities are obtained. The LDV probe volume, of approximate dimensions $\Delta X = 46$ μm, $\Delta Y = 46$ μm, $\Delta Z = 850$ μm, is located at the center of the test section of the tube, at different $X-$locations above the initial position of the nitrocellulosic membrane ($X = 0$). The fluid is seeded with 0.8 μm-diameter olive oil spherical particles. This value corresponds to the Sauter mean diameter and was measured thanks to a Spraytec Malvern system. The seeding particles response time is estimated to 1.6 μs [13]. Defining the cut-off frequency of the

particle-flow system as the fluctuation frequency of the flow velocity for which the particle response, in amplitude, has decreased by 3dB, or 30%, the particles are therefore supposed to follow velocity fluctuations over 100kHz, which gives access to most of the turbulence scales of interest in such flows. In the spatio-temporal region of interest, spanning between the incident and the reflected shock waves, LDV data rates range between 180 kHz and 550 kHz, depending on the considered flow configurations described in the next sections. The LDV measurements are triggered on the PPT2 pressure signal.

Time-resolved Schlieren visualizations are simultaneously acquired. Videos of the travelling shock wave, resulting series of compression/expansion waves and the TMZ are recorded thanks to a high-speed Phantom V12 camera. The data rate of the image recording is fixed to 27000 images per second. The characterization of the flow relies on the combined analysis of time-resolved flow visualizations, phase-averaged velocity measurements and pressure histories.

2.3 Discussion on the turbulence concept in shock tube experiments

Shock tube experiments intrinsically suffer small shock wave velocity run-to-run variations. Typical repeatability values of the shock wave velocity obtained for various shock tube setups are given in Table 1. The sources of these variations are difficult to discriminate. However in the present study, since moderate stagnation pressure changes in the driver section only weakly affect the Mach number of the shock wave and since the experimental setup is installed in a temperature-regulated room and the pressure in the driver section is controlled, the diaphragm rupture process is the most probable cause for these unpredictable Mach number run-to-run variations. This rupture process may be influenced by, *e.g.*, local defects of the diaphragm material (such as microscopic thickness variations, local prestresses or matter anisotropy, etc.), tiny variations in the manufacturing process of the fracture initiation lines used to calibrate the rupture of the diaphragm [9, 14] or small variations in the impact force of driven striking devices [9]. In the present study, the shock wave Mach number repeatability has been determined on the basis of 172 consecutive runs. It reaches 90% in the range $\pm 1\%$ of the shock wave velocity target value (412m/s for a shock wave Mach number $M = 1.2$), which represents a total of 155 validated shots. The 10% unvalidated shots correspond to prematury or partial breaking of the diaphragm and were removed from the test campaign database. In the range $\pm 0.5\%$ of the SW velocity target value, the repeatability equals 87% of the whole shots. It is still over 80% in the range $\pm 0.2\%$, corresponding to 138 shots. These correspond to 96.5% and 88.7% of the total number of validated shots considered for the present study respectively. It is thus reasonable to assume that the post-shock velocity fluctuations induced by run-to-run shock wave velocity variations should mainly be comprised in the range [105.3 m/s ; 107.65 m/s] in air (for a shock wave Mach number M=1.2, the expected velocity in shocked air is 106.2 m/s) and in the range [71.4 m/s ; 72.5 m/s] in SF_6 (the expected velocity in shocked SF_6 is 72m/s). In this work, an experiment is considered as validated when the Mach number of the incident shock wave is within the range $\pm 1\%$ of the expected value. This range was fixed as a compromise given the repeatability values reported in Table 1. However one should consider this value as overestimated since 96.5% of the runs considered for this work lie in the range $\pm 0.5\%$ and 88.7% in the range $\pm 0.2\%$ of the theoretical Mach number value. In the range $\pm 0.2\%$, the transcript of these run-to-run Mach number variations in terms of resulting velocity fluctuations in shocked air (resp. SF_6) is ± 1.45 m/s (resp. ± 0.5 m/s), or 1.36% (resp. 0.7%) of the theoretical shocked fluid velocity (106.2 m/s in air and 72 m/s in SF_6).

Ref.	*Shock tube characteristics*	*Shock wave generating device*	*M*	*Repeatability*
[15]	254mm squared cross section, WiSTL	metal diaphragm ruptured by a static cross-shaped sharp knife	1.25 - 3.08	$\pm 0.4\%$
[9]	80mm squared cross section	predetermined ruptured mylar diaphragm impacted with a driven striking pin	1.15 - 1.45	$\pm 1\%$
[14]	80mm squared cross section, IUSTI T80	predetermined ruptured steel diaphragm	1.3 - 1.5	$\pm 3\%$
[16]	127mm squared cross section, LANL VST	piston-driven driver	1.21 - 1.29	$\pm 1.6\%$
[17]	140×20 mm cross section	not communicated	1.21	$\pm 0.8\%$

Table 1. Summary of typical values of the Mach number repeatability in various shock tubes.

At this stage one can wonder the influence of such run-to-run shock wave Mach number variations on the determination of statistical quantities of interest for the study of turbulence when it is based on ensemble average of transitional flows such as the ones involved in shock tube experiments. In this context the concept of turbulence is challenging, if not partly controversial. Indeed, if one considers the incident shock wave velocity as the initial condition of the experiment, regardless of the way this shock wave is generated, then the use of the term 'turbulence' to qualify these velocity fluctuations is not appropriate since the shock wave velocity variations can not be considered as tiny. However, considering the turbulence concept at the global experimental setup level, tiny variations in the initial conditions of the shock wave generating device, induced by undetectable variations in the resistance of the diaphragm or in the force of the impacting device for instance, can lead to unpredictable perturbations leading to erratic fluctuations of the incident shock wave velocity. From the above-mentioned perspective these velocity fluctuations can then be interpreted as turbulence. Thereafter, the turbulence notion will be defined from this perspective.

3 Background turbulence of the shock tube

Before analyzing the air/SF_6 mixing configuration, the homogeneous, pure air configuration without the nitrocellulosic membrane and without mixing is first investigated. This will serve the discrimination of a potential surplus of turbulence produced in the wake of the membrane fragments from the background turbulence of the shock tube. We thus consider the following pure air configurations :

- **Conf1**: experiments with a clean test section (no grid and no nitrocellulosic membrane inside the shock tube);
- **Conf2**: experiments with two grids positioned at the interface location (bottom wire mesh with a wire spacing of 1 mm, upper wire mesh with a wire spacing of 1.8 mm), without nitrocellulosic membrane, in order to quantify the influence of the grids on the velocity turbulence levels experienced in the flow.

The schematic (X,t) diagram of these two configurations is provided in Fig. 3. The LDV probe volume is located at $X = 43$ mm above the virtual position of the nitrocellulosic membrane (not inserted in these runs). This position corresponds to the location of PPT3 pressure transducer. It thus allows us to correlate velocity and pressure histories of the main phenomena

(incident and reflected shock waves) crossing the measurement volume at a similar $X-$location. The analysis starts at the instant of passage of the incident shock wave at $X = 0$ and ends at the instant of passage of the main expansion waves in the LDV probe volume. It corresponds to the temporal window of observation used for the analysis (see Fig. 3).

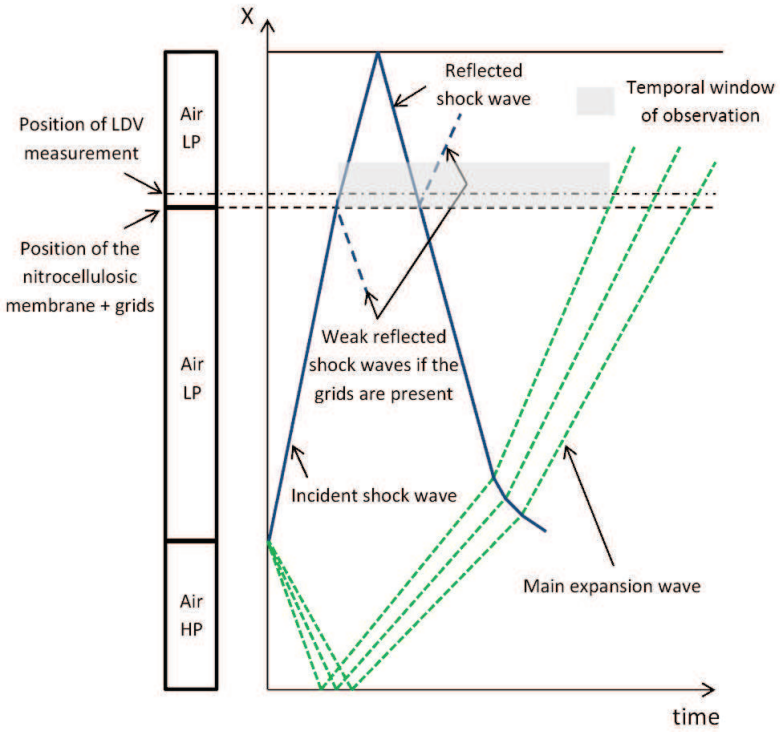

Fig. 3. Schematic $(X-t)$ diagram representative of an homogeneous experiment

For both Conf1 and Conf2 configurations, 40 experiments are conducted and the phase-averaged, mean and r.m.s. fluctuating $X-$velocities $\overline{U}$ and $\sqrt{\overline{u'^2}}$ are computed. This procedure requires a given sampling of the velocity data for the whole set of experiments, that can not be obtained from raw LDV data due to the random detection of the seeding particles in the LDV probe volume. To this avail, each velocity signal obtained from each individual experiment is sampled into a given set of time steps, relative to t_0. The width of these time steps is fixed to 10 μs around the incident and reflected shock waves and to 30 μs elsewhere. All the velocity samples obtained from the full set of experiments and contained inside a given time step are cumulated and averaged. This provides the corresponding mean and r.m.s. fluctuating velocities as a function of the time step. It has to be noticed that the width of the time steps is determined as a compromise between sufficiently high number of samples per time step (imposing a minimum temporal width), and the temporal averaging effect induced by too large time steps. Figure 4 displays typical convergence curves of the mean and r.m.s. fluctuating $X-$velocities $\overline{U}$ and $\sqrt{\overline{u'^2}}$ obtained for different time steps. It shows that sample numbers above 150 ensures the convergence of the first and second order statistics with a variance of less than 0.2% and 5% respectively. The convergence of the first order statistics still depicts a variance of less than 1% for a sample number of 100 and close to 1.5% for a sample number of 50. For the second order statistics it equals 12.5% and 30% for sample numbers of 100 and 50 respectively.

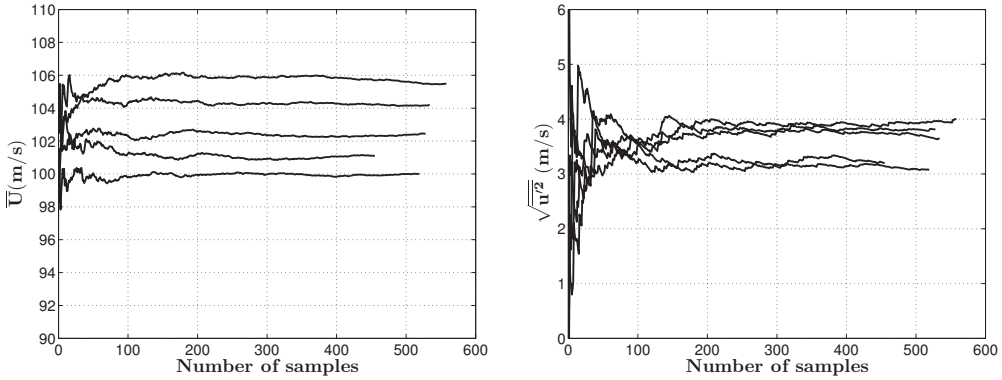

(a) (b)

Fig. 4. Convergence curves of the first and second order statistics at different time steps located between the incident and reflected shock waves, resulting from the cumulation of 40 identical experiments in pure air configuration. (a) mean $X-$velocity (b) r.m.s. fluctuating $X-$velocity.

Figure 5 reveals that the statistical convergence is reached for all the time steps ranging from $t = t_0$ (incident shock wave detected in the LDV probe volume) to $t = t_0 + 1150$ μs (reflected shock wave detected in the LDV probe volume), where high data rates are obtained from the LDV measurements. Beyond this range, the data rates drastically decrease due to lower velocities. This leads to a number of samples below the convergence threshold. However one can notice that the global evolution of the mean and r.m.s. fluctuating velocity histories remains consistent with the converged part of the curves in these regions of coarser convergence.

Figure 5(a) depicts time evolutions of $\overline{U}$ for the two previously described flow configurations. Corresponding PPT3 pressure signals are illustrated on Fig. 6, and Fig. 7 shows the simultaneously acquired Schlieren images. Interestingly enough, those images reveal a complex acoustic field in the wake of the incident shock wave, comprising series of compression/expansion non planar waves. Those waves are induced by the travelling of the shock wave over slight parietal defaults, in the form of steps a few tens of micron deep, at the junction of the different modules constituting the tube. The analysis of the time evolution of $\overline{U}$ for the first configuration Conf1 reveals the progressive increase of the mean velocity level from $\overline{U} \approx 100$ m/s to $\overline{U} \approx 106$ m/s which corresponds to the expected velocity behind the M=1.2 incident shock wave. This progressive increase of the mean velocity results from the combined effect of the above-mentioned acoustic field in the wake of the incident shock wave and from the development of the boundary layers on the walls of the test section. The time evolution of $\overline{U}$ is also characterized by slight oscillations whose periods are in good agreement with both the PPT3 pressure signals (Fig. 6) and the tracks of the previously evoked series of compression/expansion waves clearly observable on the Schlieren images (Fig. 7).

The analysis of the history of $\sqrt{\overline{u'^2}}$ for Conf1 (Fig. 5(b)) reveals the concomitant increase of $\sqrt{\overline{u'^2}}$ with $\overline{U}$. It reflects the nearly constant turbulent activity of the flow between the incident and reflected shock waves. Thus the values of both the r.m.s. fluctuating $X-$velocity and the associated turbulence intensity, hereafter denoted $(\sqrt{\overline{u'^2}},\ \sqrt{\overline{u'^2}}/\overline{U})$ equal $(3.2\ \mathrm{m/s}, 3.2\%)$ just after the passage of the incident shock wave in the LDV probe volume, at $t = t_0$, and $(3.8\ \mathrm{m/s}, 3.6\%)$ just before the passage of the reflected shock wave in the LDV probe volume, at $t = t_0 + 1.2$ ms. As mentioned in section 2.3, run-to-run SW velocity variations are partly responsible for these velocity fluctuations. However this does not fully explain

the actual fluctuation levels, since it is over twice the fluctuation values attributed to run-to-run SW velocity variations. The influence of the complex acoustic field observed through both Schlieren visualizations and pressure measurements can thus be considered as partly responsible for the measured velocity fluctuations.

For Conf2, while the time evolution of the mean velocity $\overline{U}$ is analogous to Conf1, the history of the r.m.s. fluctuating velocity $\sqrt{\overline{u'^2}}$ notably differs and reveals the influence of the grids on the fluctuation levels experienced by the flow. Two distinct levels are thus observed between the incident and reflected shock waves. The first one, spanning between $t = t_0$ and $t = t_0 + 430$ μs, reflects the turbulent properties of the fluid initially located above the grids and equals $(3.2 \text{ m/s}, 3.2\%)$. As expected, this is in good accordance with Conf1 since this volume of fluid has undergone a similar history. The second level depicts fluctuating values of about $(4.97 \text{ m/s}, 4.7\%)$ and corresponds to the fluid that has crossed the grids. The comparison of these values with the ones obtained for Conf1 just before the passage of the reshock reveals that the presence of the grids is responsible for a 1.1% increase of the turbulent intensity.

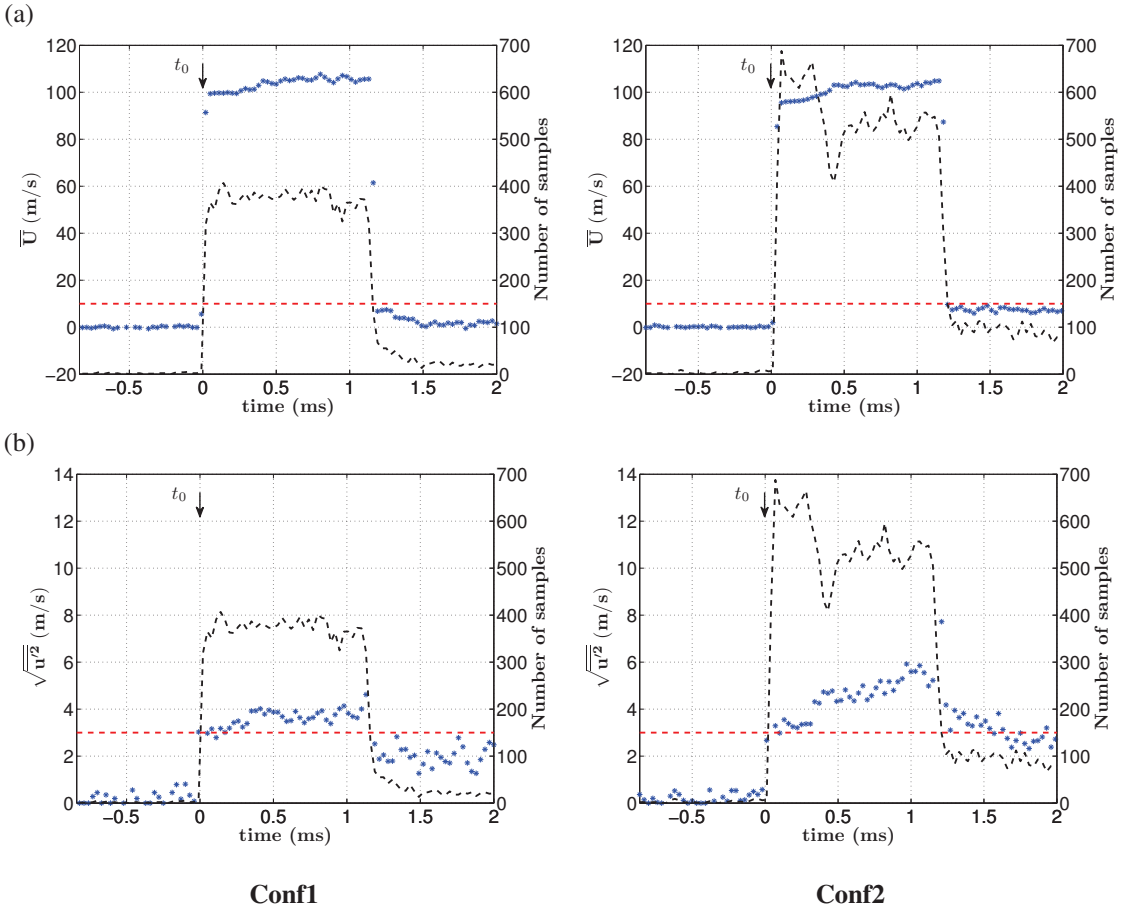

Fig. 5. Evolution of (a) the mean $X-$velocity $\overline{U}$ and (b) the r.m.s. fluctuating $X-$velocity $\sqrt{\overline{u'^2}}$ (blue symbols, left vertical axis) - Conf1 (left) and Conf2 (right). Number of samples used for the calculation of the statistics on each time step of the discretized velocity signal (black dashed line, right vertical axis). The red horizontal line corresponds to the number of samples necessary to get convergence. The origin of time on the figure corresponds to the instant of passage t_0 of the incident shock wave on the LDV probe volume at $X = 43$ mm.

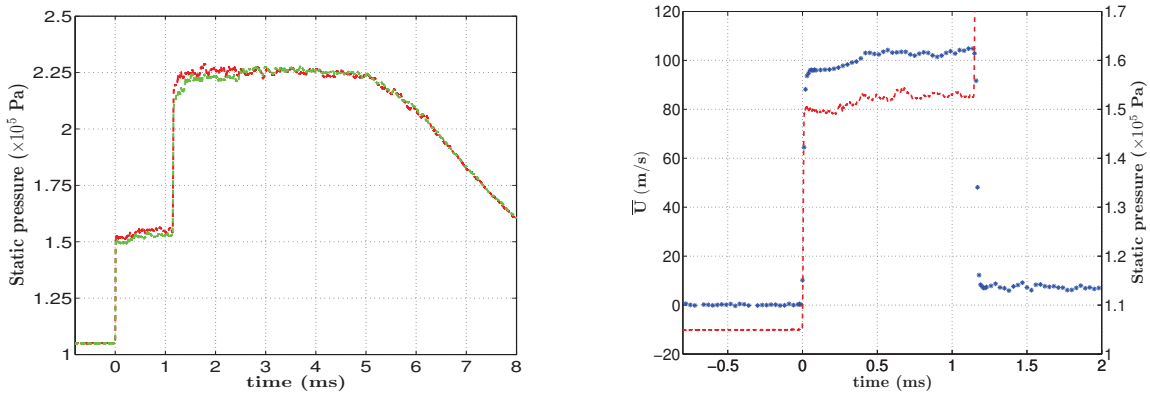

(a) (b)

Fig. 6. (a) PPT3 static pressure signals (X=43 mm above the interface) for Conf1 (green) and Conf2 (red) over the whole phenomenon history ; (b) Concurrent evolutions of the mean $X-$velocity (blue symbols) and PPT3 static pressure (red dashed line), zoomed around the velocity plateau between the incident and reflected shock waves for Conf2. The origin of time on the figure corresponds to the instant of passage t_0 of the incident shock wave on the LDV probe volume at $X = 43$ mm.

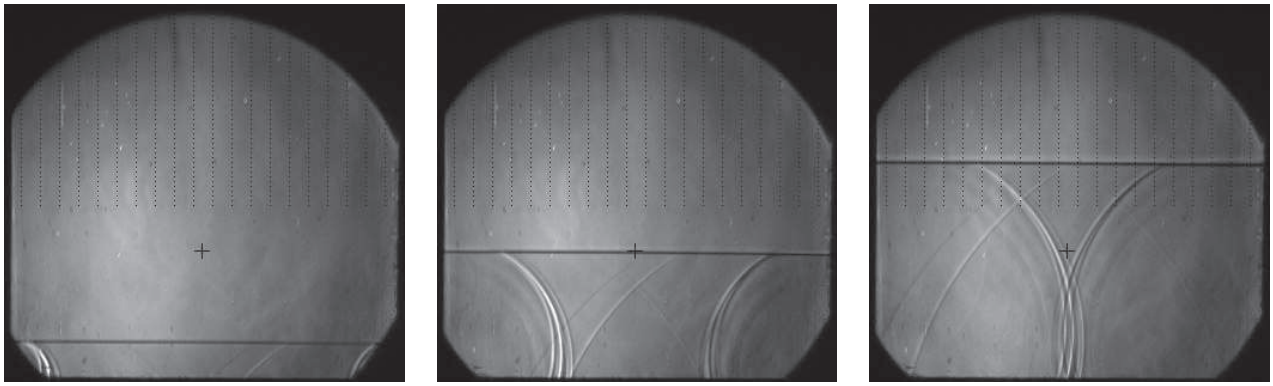

$t = t_0 - 74.1\ \mu$s $t = t_0$ $t = t_0 + 74.1\ \mu$s

Fig. 7. Schlieren images of the perturbations generated by the shock wave in pure air (Conf1). The black cross on the images indicates the location of the LDV probe volume at $X = 43$ mm. The origin of time on the figure corresponds to the instant of passage t_0 of the incident shock wave on the LDV probe volume.

4 Influence of the membrane fragments in pure air configurations

Here the intermediate situation between an homogeneous flow, with and without the presence of the grids (Conf1 and Conf2), and air/SF_6 mixing configurations is investigated. We consider a flow configuration similar to Conf2 (presence of the two grids) to which the nitrocellulosic membrane is added. The objective is to estimate the influence of the membrane fragments generated by the passage of the incident shock wave across the membrane on the turbulent levels experienced in the test section. This will serve the discrimination of the turbulence level produced by the mixing of the two gases in the TMZ, through baroclinic effects, from the background turbulence of the experimental setup. The corresponding set of experiments will be hereafter denoted **Conf3**.

4.1 Analysis of the measurements

As in the preceding configurations, 40 experiments are phase-averaged in order to get velocity statistics. The corresponding results are shown in Fig. 8. The statistics are converged between the incident and reflected shock waves except when large membrane fragments temporarily cross the LDV probe volume, partially cutting the Doppler signals between $t = t_0 + 260\ \mu$s and $t = t_0 + 560\ \mu$s ('blackout' phenomenon inducing the strong decrease of the number of samples available for LDV measurements). These fragments are clearly visible on the Schlieren images of Fig. 9. This result demonstrates the impact of the membrane fragments on the convergence of the phase-averaged statistics. Considering the low number of LDV samples obtained in the time steps affected by the presence of the fragments (a minimum of 20 samples is measured at $t \approx t_0 + 380\ \mu$s, at mid-time of the blackout), the required number of experiments necessary to attain the convergence threshold can be estimated to no less than 280 in this region. However, despite this observation and the low number of samples between $t = t_0 + 260\ \mu$s and $t = t_0 + 560\ \mu$s, the evolutions of $\overline{U}$ and $\sqrt{\overline{u'^2}}$ still appear consistent with the two surrounding statistically converged regions. This is finally quite logical, given the typical convergence histories illustrated in Fig. 4, where the converged values are expected to be reasonably approached with a limited number of samples, beyond 30.

Figure 8(a) shows that the phase-averaged mean velocity is not affected by the presence of the membrane (and by the resulting fragments). It depicts perfectly similar time evolution in comparison with Conf1 and Conf2. The phase-averaged history of the r.m.s. fluctuating $X-$velocity $\sqrt{\overline{u'^2}}$ measured for Conf3 is depicted in Fig. 8(b). As for Conf2, two consecutive turbulence levels are observed between the incident and the reflected shock waves. The first one is similar to Conf1 and Conf2 $(3.2\ \mathrm{m/s}, 3.2\%)$, whereas the second one is close to $(7.5\ \mathrm{m/s}, 7\%)$, which corresponds to a further increase of 2.3% induced by the membrane fragments (in comparison with the 4.7% second turbulence level measured for Conf2). This increase is concomitant with the passage of the fragments inside the LDV probe volume depicted on the time-resolved images (Fig. 9). It can thus be concluded that the membrane fragments not only hinder the convergence of the velocity statistics when they cross the LDV probe volume, but also produce a non-negligible surplus of turbulence.

At last, just after reshock (beyond $t = t_0 + 1.2$ms), one can observe an additional increase of the r.m.s. fluctuating $X-$velocity. Two contributions can be identified in order to explain this post reshock increase of $\sqrt{\overline{u'^2}}$. First the well-documented shock-turbulence interaction process is responsible for an amplification of the pre reshock fluctuating levels (see *e.g.* [18]). Second, the transient relative-to-surrounding fluid motion of the fragments is re activated during the reshock process, which induces the transient generation of wake agitation as detailed below.

4.2 Discussion on the fragment-induced velocity fluctuations

The influence of the membrane fragments on the production of velocity fluctuations is a complex issue. It depends on the coupling between the dynamics of the fragments and the surrounding flow. This coupling is in turn influenced, amongst others, by the ability of the fragments to respond to the various time scales of the flow. Two critical time scales can be identified: one corresponding to the discontinuity induced by the shock wave passage, another one associated with flow structures whose size is of the same order as the one of the fragments and which can be assimilated to the smallest continuous flow time scale able to affect the mean dynamics of fragments. The response time of the fragments itself depends on their

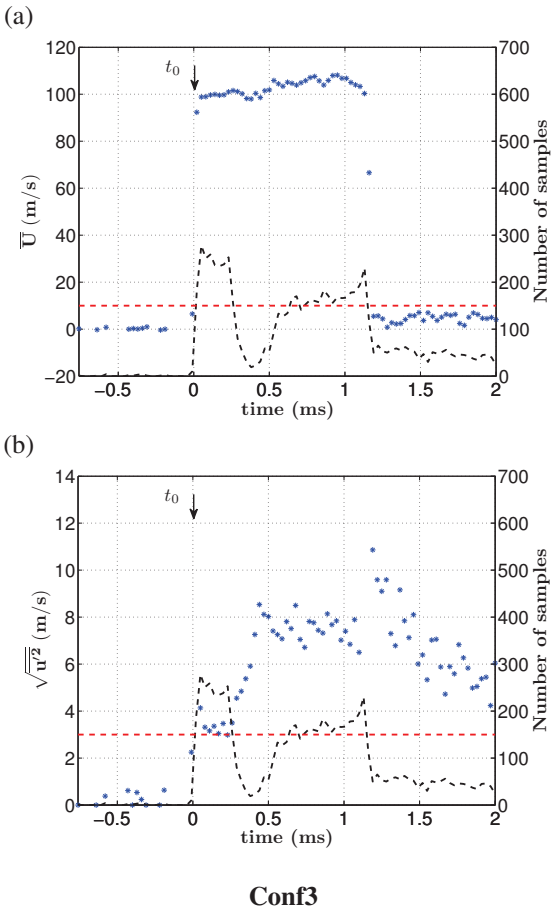

Fig. 8. Evolution of (a) the mean $X-$velocity $\overline{U}$ and (b) the r.m.s. fluctuating $X-$velocity $\sqrt{\overline{u'^2}}$ (blue symbols, left vertical axis) - Conf3. Number of samples used for the calculation of the statistics on each time step of the discretized velocity signal (black dashed line, right vertical axis). The red horizontal line corresponds to the number of samples necessary to get convergence. The origin of time on the figure corresponds to the instant of passage t_0 of the incident shock wave on the LDV probe volume at $X = 43$ mm.

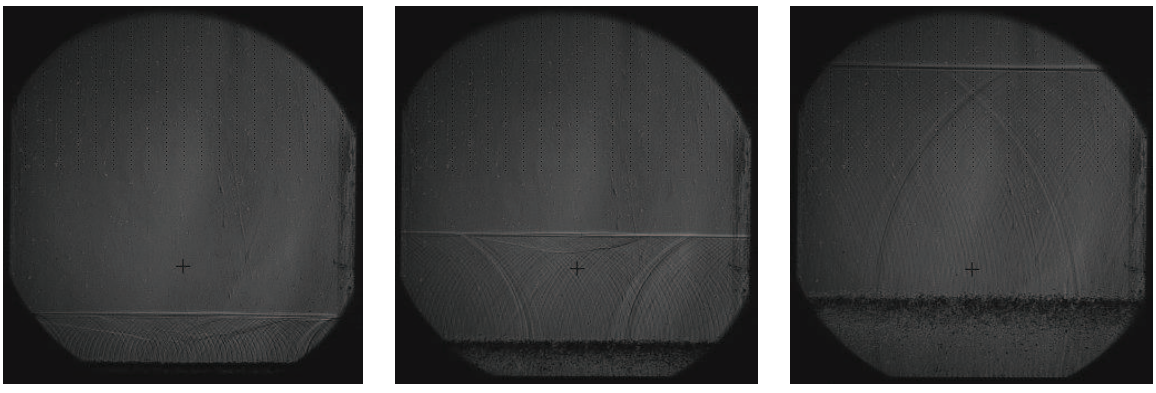

$t = t_0 - 44\ \mu$s $\qquad$ $t = t_0 + 30.1\ \mu$s $\qquad$ $t = t_0 + 178.2\ \mu$s

Fig. 9. Schlieren images of the perturbations generated by the shock wave in pure air configuration (Conf3). The black cross on the images indicates the location of the LDV probe volume at $X = 43$ mm. The origin of time on the figure corresponds to the instant of passage t_0 of the incident shock wave on the LDV probe volume. Here the dark zone corresponds to membrane fragments.

size (affected by the mesh size of the upper grid), shape (affecting the drag coefficient of the fragment), density relative to the surrounding fluid density, and on the surrounding fluid properties (density, viscosity). The precise determination of this

response time is a priori out of reach since the abovementioned parameters are partly unknown. However the analysis of time-resolved Schlieren images obtained for Conf3 indicates that the membrane fragments reach a similar-to-surrounding fluid velocity (in other words that their slipping velocity tends to 0) in a time interval close to the one separating 2 consecutive images ($37\mu s$).

5 Velocity fluctuations in mixing configurations

The final step of the analysis is conducted in this section by considering an air/SF_6 mixing case, hereafter denoted **Conf4**. As already mentioned in section 2, the experimental setup and procedure are the same as in pure air configurations with identical parameters for the flow ($L = 250$ mm, thin nitrocellulosic membrane trapped between the two previously described grids, incident shock wave Mach number of 1.2 travelling from the light gas towards the heavy gas, Atwood number of 0.67). A schematic (X,t) diagram of the mixing cases is given in Fig. 10. This diagram also depicts the temporal window of observation that will be used for the analysis. It starts at the moment of the interaction of the incident shock wave with the initial gaseous interface, referred to as the time origin $t = 0\ \mu$s, and ends at the moment of the interaction of the main expansion waves with the TMZ. The origin of time is thus fixed regardless of the LDV measurement station. t_0 still refers to the instant of passage of the transmitted shock wave in the LDV probe volume. In this temporal window of observation, a sequence of time-resolved Schlieren images is given in Fig. 11 as an illustration of the RMI-induced mixing process.

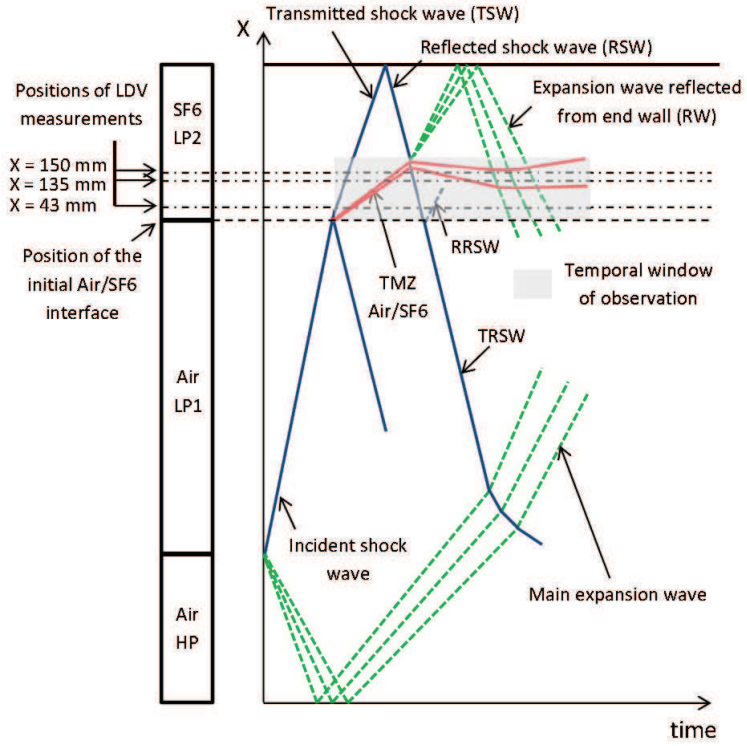

Fig. 10. Schematic $(X-t)$ diagram of an Air/SF_6 experiment. Except for the previously defined TMZ acronym, letters W, T and R used in the acronyms refer to 'wave', 'transmitted' and 'reflected' respectively.

Three LDV measurement $X-$locations are chosen above the initial position of the nitrocellulosic membrane for the

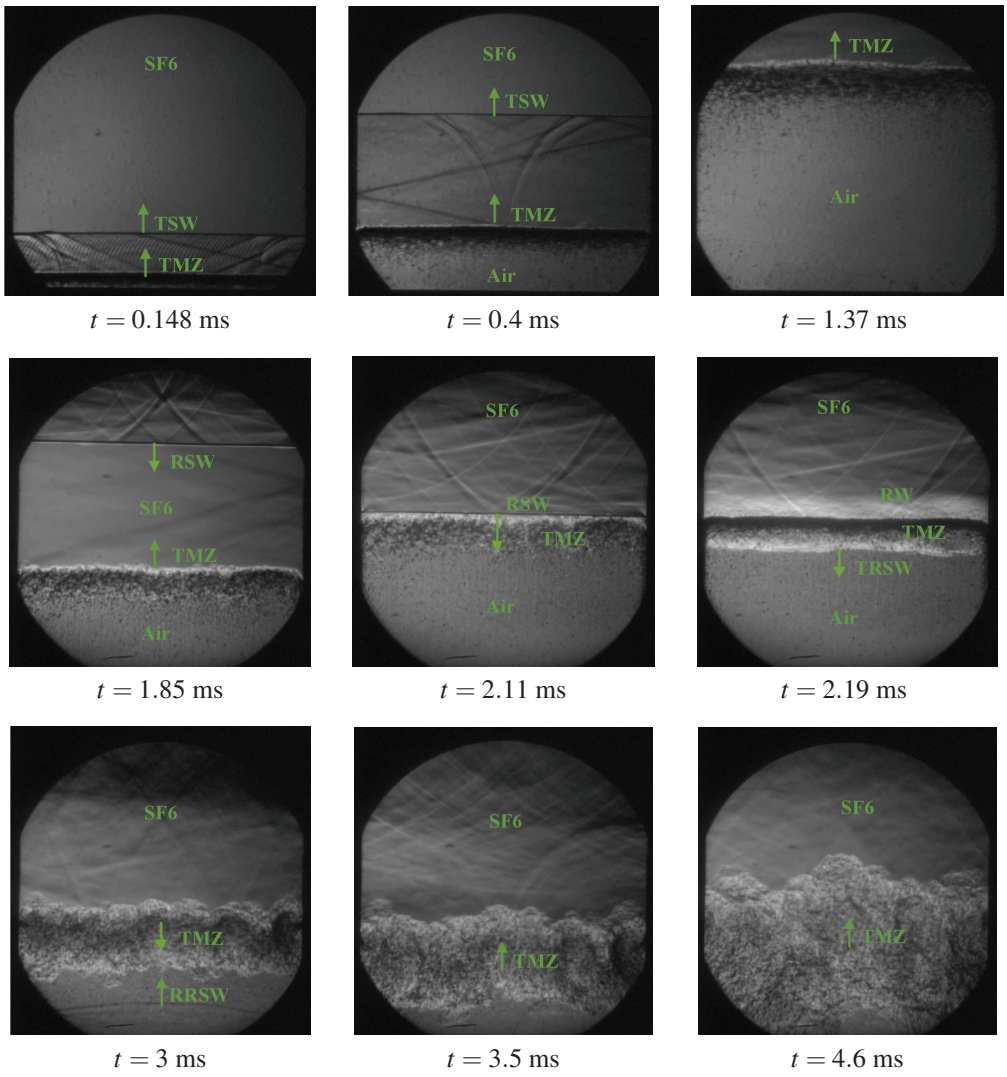

Fig. 11. Illustration of the TMZ evolution (Conf4). The reader can refer to Fig. 10 for the definition of acronyms.

analysis of the TMZ evolution. The first position, corresponding to $X = 43$ mm, allows a direct comparison of the mixing configuration with pure air configurations. It also gives access to the early stage of development of the ascending TMZ. Since the interaction of a developed TMZ with a reshock is of prime interest for this study, two additional LDV measurement stations, located at $X = 135$ mm and $X = 150$ mm respectively, are also investigated. Indeed the analysis of the $(X-t)$ diagram (schematic illustration given in Fig. 10. See also Fig. 14 for an illustration of the actual, experimentally determined, $(X-t)$ diagram) shows that the TMZ boundaries remain confined in the range $X \in [120\text{ mm}, 155\text{ mm}]$ for instants ranging between the interaction of the reflected shock wave (RSW) and the reflected expansion waves (RW) with the TMZ. As such the $X = 135$ mm station is chosen as a median position inside the above-mentioned range. The $X = 150$ mm station, which corresponds to the highest position below the cusp of the TMZ trajectory, allows to scan the entire TMZ, from its upper to its lower boundaries (in the previously defined time interval).

For each of these LDV measurement stations, 35 experiments are phase-averaged following the same procedure as described in section 3. The convergence threshold remains of the same order as the one observed in pure air cases, *i.e.* 150 samples per time step to reach full convergence.

Figure 12, left-hand column, displays instantaneous LDV measurements for the three $X-$locations. For an incident Mach number of 1.2 in the air, the SF_6-transmitted shock wave accelerates the flow to $\overline{U} \approx 73.5$ m/s until the arrival of the reflected shock wave. In addition time-resolved Schlieren images (not depicted in Fig. 12, for the sake of consiceness) indicate that, for the LDV measurement station $X = 43$ mm, the TMZ is located below the LDV probe volume at $t = 555$ μs and above it at $t = 592$ μs. During this time interval, the mean velocity of the flow still equals $\overline{U} \approx 73.5$ m/s (Fig. 12). Consequently, for $X = 43$ mm, the ascending TMZ is assumed to travel at $\overline{U} \approx 73.5$ m/s and to cross the LDV probe volume as from $t = 585$ μs (*i.e.* 585 μs after the passage of the transmitted shock wave through the initial gaseous interface). At that time, the thickness of the TMZ is estimated to $h = 7$ mm, based on Schlieren images. This value was obtained from a specific image post-processing, based on the use of frequential filters. It consists in first, applying a 2D Fast Fourier Transform (FFT) on the raw images, second high-pass filtering the previously transformed images in order to eliminate the low frequency components of the image associated with the homogeneous zones, last applying the inverse FFT, revealing the boundaries of the TMZ. This technique is detailed in [19]. Therefore, the crossing of the TMZ through the LDV probe volume, illustrated on Fig. 12, is expected to last 95 μs. From Fig. 12(a), the duration of the 'blackout' (Doppler signal cut) can be estimated to 320 μs and starts at the instant of passage of the upper boundary of the TMZ in the LDV probe volume. We can thus conclude that membrane fragments still cross the LDV probe volume after the passage of the TMZ, partially cutting the Doppler signals for an additional time duration of 225 μs. This conclusion is further supported by the Schlieren image presented in Fig. 13. On both sides of the blackout, reasonable LDV data acquisition rates are obtained (180 kHz in pure SF_6 before the blackout and 320 kHz in pure air after the blackout). However, this data rate is drastically reduced as long as membrane fragments are crossing the LDV probe volume. The same observations can be made for the instantaneous velocities measured for the two other locations. For $X = 135$ mm, Fig. 12(b) displays two consecutive blackouts. The first one lasts about 400 μs and corresponds to the ascending TMZ. The second one corresponds to the re-shocked TMZ (after the cusp of its trajectory, see Fig. 10). Its duration, much longer than the previous one, is estimated to 4.72 ms. This indicates that most of the membrane fragments lag inside and behind the re-shocked stagnating TMZ. For $X = 150$ mm, Fig. 12(c) depicts a unique, long blackout of approximately 1.32 ms. For this specific measurement station, the LDV probe volume is close to the cusp of the TMZ. The membrane fragments tend to stagnate around the measurement zone such that the incident and reflected phases can not be discriminated.

The corresponding mean $X-$velocity temporal evolutions obtained by averaging over the 35 experiments are displayed in Fig. 12, right-hand column. The gases are first accelerated to $\overline{U} \approx 73.5$ m/s after the interaction of the incident shock wave with the initial interface, then slow down to $\overline{U} \approx -18$ m/s after TMZ/reflected shock wave (RSW) interaction, and are finally accelerated once again to $\overline{U} \approx 5$ m/s after the arrival of the reflected expansion waves RW (see. Fig. 10). At late times of the temporal window of observation, after $t = 5$ ms, the main expansion waves coming from the bottom of the shock tube reach the test section and decelerate the flow to $\overline{U} \approx -20$ m/s. Similarly to pure air configurations, the convergence rate of the statistics falls below the required threshold when membrane fragments cross the LDV probe volume. For $X = 43$ mm, the number of samples available in the different time steps is very similar to what has been reported for Conf3 (pure air + membrane), whereas a worst situation is observed for $X = 135$ mm where the number of samples remains close to zero for

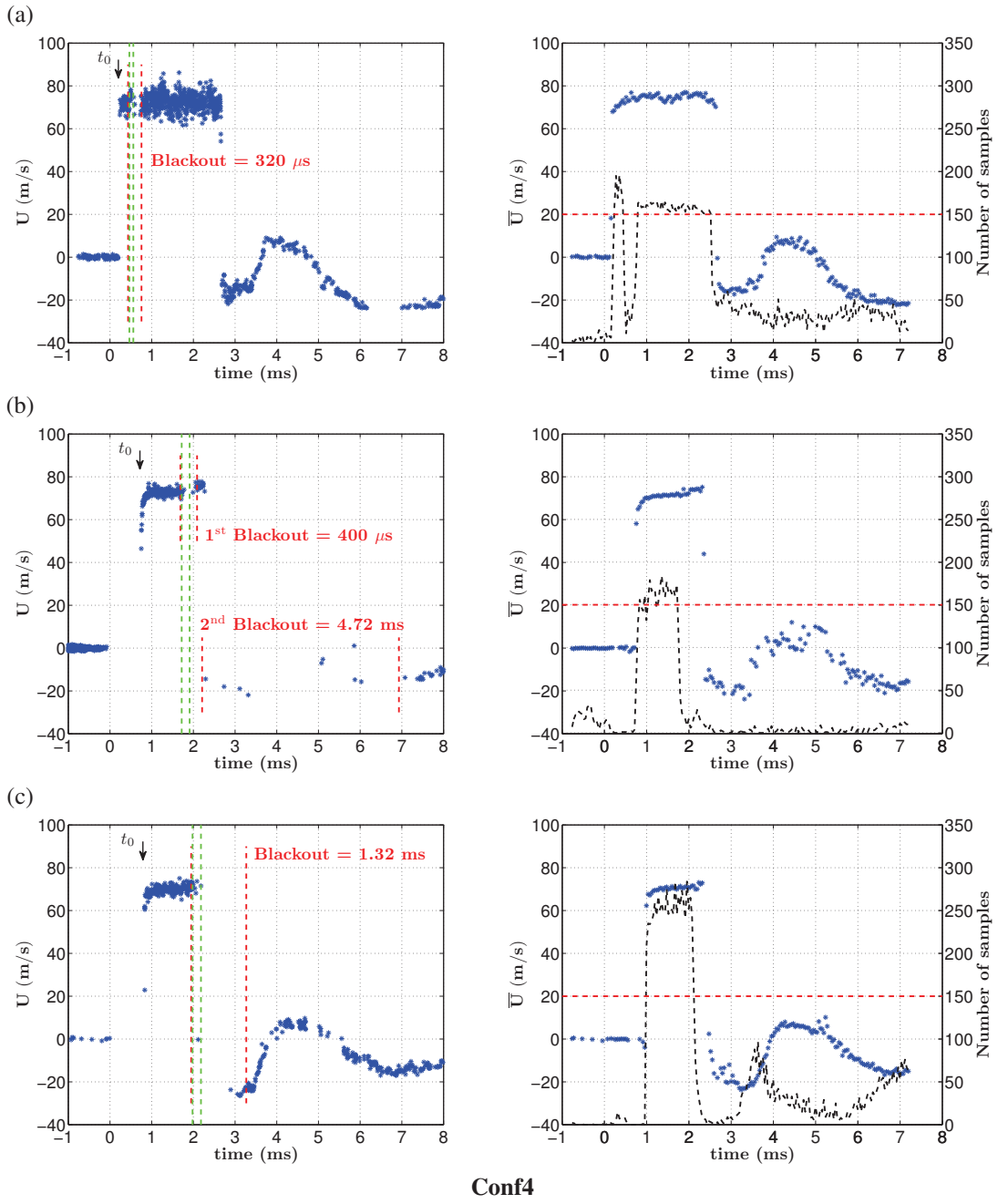

Fig. 12. Conf4: LDV measurements of the instantaneous (left-hand column) and mean (right-hand column) $X-$velocity U and $\overline{U}$ for the 3 locations (a) $X = 43$ mm, (b) $X = 135$ mm, (c) $X = 150$ mm. t_0 corresponds to the instant of passage of the incident shock wave on the LDV probe volume. (Left-hand column): Green dashed lines correspond to the temporal location of the TMZ. Red dashed lines depict the temporal location of the blackout. (Right-hand column): number of samples used for the calculation of the statistics on each time step of the resampled velocity signal (black dashed line, right vertical axis). The red horizontal line corresponds to the number of samples necessary to get convergence.

all the instants consecutive to the passage of the ascending TMZ. This measurement station, located close to the center of the stagnating TMZ, thus appears particularly inappropriate for LDV measurements in RMI-induced mixing configurations since the membrane fragments remain confined inside the TMZ in this region of evolution. The analysis seems however more promising for $X = 150$ mm since the number of samples recovers non-negligible values after reshock, between 3.2 and 4 ms, even if the convergence threshold is still not reached. This effect can be attributed to the distance separating the

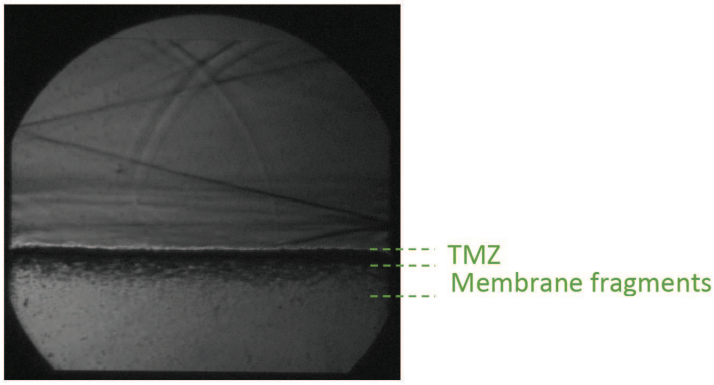

Fig. 13. Visualization of the ascending TMZ in its early stage of development and of the following membrane fragments (Conf4)

LDV probe volume from the initial gaseous interface. For large enough LDV probe location-to-inital interface distances, the inertia of the membrane fragments allows to partly separate them from the core of the TMZ. This leads to a lower fragment concentration in the region of interest, and thus to improved data rates for the LDV measurements. Consequently this tends to improve the convergence. For the remaining time steps affected by the blackout, where the number of samples is particularly low, a proper convergence can not be expected, even for a repetition of a very large number of identical experiments.

In light of the previous considerations about the actual convergence rate of the LDV measurements in mixing configuration, r.m.s. fluctuating $X-$velocities should only be quantitatively analysed in the temporal regions located between the incident and reflected shock waves, where the convergence threshold is globally reached (except during the passage of the TMZ where the data rate drastically falls). The values of the corresponding turbulent fluctuations and intensities are gathered in Fig. 14 which provides a complete time-space picture of the measured turbulent properties of the RMI-induced mixing history.

Between the passage of the incident shock wave and the crossing of the TMZ in the LDV probe volume, in pure SF_6, the fluctuating values $(\sqrt{\overline{u'^2}}, \sqrt{\overline{u'^2}}/\overline{U})$ equal $(3.1\ \mathrm{m/s}, 4.2\%)$, $(2.25\ \mathrm{m/s}, 3.1\%)$ and $(2\ \mathrm{m/s}, 2.7\%)$ for LDV measurement stations $X = 43$ mm, $X = 135$ mm and $X = 150$ mm respectively. One can notice that the background turbulence initiated in the SF_6 by the transmitted shock wave and the refracted compression waves (visible in Fig. 11 at $t = 0.148$ ms) gradually decrease with the measurement location. Interestingly enough, considering r.m.s. fluctuating $X-$velocities at $X = 43$ mm (unique common measurement station between pure air and mixing configurations), one can notice similar values for both Conf3 and Conf4, close to 3.2 m/s in pure air and 3.1 m/s in pure SF_6 respectively, before the arrival of the TMZ. This tends to indicate that the incident shock wave and consecutive refracted waves induce similar turbulent agitation in both pure air and pure SF_6. However the transcript of this agitation in terms of turbulent intensity is different for Conf3 and Conf4: they are estimated to 4.2% in pure SF_6 (Conf4) and 3.2% in pure air (conf3) at $X = 43$ mm. This reflects the lower mean $X-$velocity in SF_6 in comparison with air – 73.5 m/s in SF_6 instead of 106 m/s in pure air – see sections 3 and 4.

After the passage of the TMZ up to the reflected shock wave, in pure air, the fluctuating values $(\sqrt{\overline{u'^2}}, \sqrt{\overline{u'^2}}/\overline{U})$ are equal to $(5\ \mathrm{m/s}, 6.8\%)$ for $X = 43$ mm and $(2.18\ \mathrm{m/s}, 2.96\%)$ for $X = 135$ mm. Note that for $X = 150$ mm, no fluctuating values can be calculated in pure air due to the too short time interval between the consecutive passages of the ascending

and descending TMZ in the LDV probe volume (see Fig. 14). Here, considering the measurement station $X = 43$ mm, the turbulent intensity is nearly the same for both Conf3 (7%) and Conf4 (6.8%). Regarding the normalized decay laws of grid-generated turbulence [20], this result is consistent since for both Conf3 and Conf4, the volume of fluid (pure air initially located below the gaseous interface) crossing the measurement zone has experienced analogous histories.

During the passage of the TMZ in the LDV probe volume, we remind that the convergence threshold is not strictly reached. However and as mentioned in sections 3 and 4, given the typical convergence histories illustrated in Fig. 4, the converged value is expected to be reasonably approached with a limited number of samples, beyond 30. In that sense we consider as appropriate to provide the following values as an indicator of the turbulent levels inside the TMZ before its interaction with the reflected shock wave. For LDV measurement station $X = 43$ mm the fluctuating values are estimated to $(3.6\ \mathrm{m/s}, 4.9\%)$ inside the TMZ. These values are slightly higher than the ones measured in pure SF_6 before the passage of the TMZ. This increase can be attributed, without pre-empting their relative proportion, to both the baroclinic RMI-induced mixing and the velocity fluctuations produced in the wake of membrane fragments. Unfortunately it is not possible to discriminate their relative contribution since, as previously mentioned, a large number of membrane fragments still lag inside the greater part of the TMZ. For higher measurement locations, the fluctuating values progressively decrease with the distance from the initial interface, under diffusive effects. These values equal $(2.4\ \mathrm{m/s}, 3.3\%)$ for $X = 135$ mm and $(2.1\ \mathrm{m/s}, 2.9\%)$ for $X = 150$ mm. It is interesting to note that this trend is similar to the observations of Poggi *et al.* [8] for an Atwood number of -0.67 (corresponding to an incident shock wave travelling from SF_6 to air).

After the interaction of the TMZ with the reflected shock wave, the statistical convergence threshold is no more reached, whatever the above-mentioned LDV measurement station. However, for the measurement station $X = 150$ mm, the number of samples temporarily rises up to ≈ 50 when the upper part of the descending, reshocked TMZ crosses again the LDV probe volume, between $t = 3.2$ ms and $t = 4$ ms (see Fig. 12). Here the measured value of the turbulent agitation $(\sqrt{\overline{u'^2}}, \sqrt{\overline{u'^2}}/\overline{U})$ equals $(3.5\ \mathrm{m/s}, 15.7\%)$. These values can thus be considered as indicative of the fluctuating levels inside the reshocked TMZ. Comparing these values with the fluctuating levels measured inside the ascending TMZ $(2.1\ \mathrm{m/s}, 2.9\%)$, just before reshock at the same location $X = 150$ mm, a 1.4 m/s increase of the fluctuating velocity is noticed. As for the associated turbulence intensity, its dramatic increase also results from the strong decrease of the norm of the mean velocity. The increase of the fluctuating levels is expected in the re-shocked TMZ since a new amount of energy is injected in the mixing zone by the reflected shock wave, and the baroclinic vorticity source term is re-activated. Finally the observed difference in the fluctuating levels in the TMZ before and after reshock is also probably due, to a lesser extent, to the additional artificial mixing induced by the fragments in their wake. In the present experimental configuration it is not possible to strictly discriminate the contribution of the membrane fragments from the contribution of the RMI-induced baroclinic terms to the measured fluctuating levels. One can at best speculate about their relative contribution taking advantage of the characterization conducted in pure air cases (Conf3). As mentioned in section 4.2, the fragment-induced velocity fluctuations originate from the wake that is transiently generated downstream of the fragments, when their slipping velocity relative to the surrounding fluid is still noticeable. Once the slipping velocity of the fragments approaches 0, the wake generation and the resulting production of velocity fluctuations stop while the transiently generated wake decays. At the instant of maximum slipping velocity (such

as at the instant of passage of the shock wave), the Reynolds numbers of the fragments in pure SF6 and pure air, and as a consequence in the intermediate TMZ case, all lie in the range of moderate Reynolds number values, for which the turbulent wake depicts similar topology and turbulent intensity levels. Moreover, the higher density value of the SF6 in comparison with air suggests a shorter time response of the fragments in pure SF6, and consequently in the mixing zone, of intermediate density. One can thus infer similar, if not smaller fragment-induced fluctuation levels in the mixing zone and in pure SF6 than in pure air.

This phenomenon is illustrated if Fig. 15, for an experimental configuration involving an upper grid of mesh-spacing equal to 12.1 mm. It should be noticed that this specific grid imposes much larger membrane fragments than the ones generated in the configurations investigated here. It depicts the rear boundary of the TMZ after reshock, where pockets of fluid are extracted from the mixing zone by large 'spoon-shaped' membrane fragments (their size is estimated to be close to the mesh spacing of the grid, *i.e.* $\sim$ 12 mm). These mechanisms are also certainly active in Conf4 inside the TMZ, but to a lesser extent since the membrane fragments are much smaller ($\sim$ 1 mm), leading to a slight over-production of turbulent agitation.

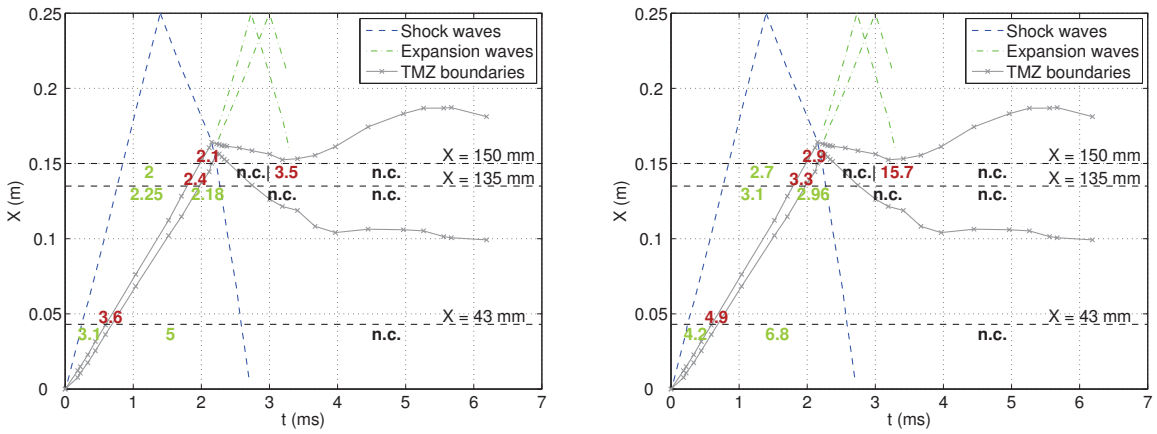

(a) (b)

Fig. 14. Experimental $(X-t)$ diagram of an Air/SF_6 mixing configuration (Conf4) and associated measured (a) fluctuations (m/s), (b) turbulence intensity ($\%$). Green and purple numbers correspond to statistically converged or indicative values of the turbulence levels respectively. 'n.c.' refers to non-converged values.

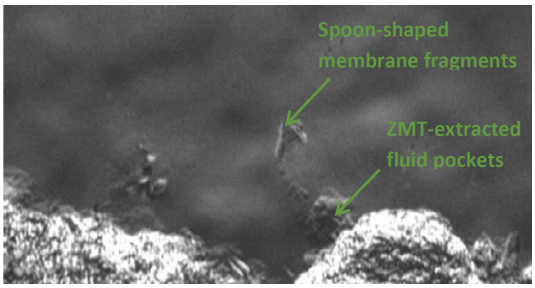

Fig. 15. Illustration of the influence of the nitrocellulosic membrane on the flow. Zoom of the TMZ rear-boundary after reshock. In the experiment illustrated in this figure, the upper grid was replaced by a grid of mesh-size 12.1mm, leading to the generation of large size membrane fragments. All the other experimental parameters were kept identical to Conf4 parameters.

6 Summary

In this paper we have experimentally investigated the late development of a Richtmyer-Meshkov instability-induced turbulent mixing zone and its subsequent evolution after the reshock phenomenon. Here the initial interface separating the two gases of different densities is obtained thanks to a thin nitrocellulosic membrane trapped between two grids. On the basis of coupled Laser Doppler Velocimetry measurements, wall pressure histories and time-resolved Schlieren images, 4 configurations were analysed, aiming at discriminating 1) background, 2) grid-induced, 3) membrane fragments and mixing-produced turbulence.

To this avail three pure air configurations were first investigated. The first one has revealed the background turbulent intensity of the shock tube, around 3.6%. Complementary investigations have highlighted the influence of the grids and the membrane fragments on the surplus of turbulence intensity measured in the test section, of the order of 1.1% for the grids and 2.3% for the membrane fragments. These preliminary studies have demonstrated that 150 Laser Doppler Velocimetry samples per time step, corresponding to the repetition of 40 identical experiments, were necessary to ensure the statistical convergence of the mean and fluctuating velocities outside the membrane fragments-polluted region. Moreover it has been shown that the satisfaction of the convergence threshold inside the polluted region would require up to 280 identical experiments.

The mixing configuration investigated in a second phase has emphasized the difficulties in reaching fully converged statistics for the complete history of the phenomenon. In particular it has been shown that the presence of a large number of membrane fragments in the core and in the periphery of the turbulent mixing zone strongly hinders the achievement of velocity measurements when these fragments cross the region of interest, causing a ‘blackout phenomenon’, even if hundreds of identical experiments were to be cumulated. These convergence difficulties are however not of the same importance depending on the measurement location above the initial gaseous interface. Thus the Laser Doppler Velocimetry measurement stations located far enough from the initial interface, and in particular just below the cusp of the turbulent mixing zone trajectory, have been identified to be less affected by membrane fragments than lower measurement stations, since the fragments inertia tends to separate them from the core of the mixing zone. For these sufficiently distant measurement locations, pertinent velocity measurements are thus obtained in the mixing zone after reshock, where the cumulated number of samples temporarily rises up to noticeable levels. These levels, if still below the strict convergence threshold, allow to extract mean-

ingful trends for the mean and fluctuating velocity levels. In particular, the reshock induces a 50% increase of the root mean square fluctuating velocity while the norm of the mean velocity dramatically decreases. This turbulence increase reveals the new amount of energy injected in the mixing zone by the reflected shock wave and the action of baroclinic vorticity source terms.

Acknowledgements

This work is supported by CEA, DAM, DIF under grant number 09-37-C-SACO monitored by Dr. Denis Souffland.

References

[1] Taylor, G., 1950. "The instability of liquid surfaces when accelerated in a direction perpendicular to their planes". *Proc. R. Soc. A,* **201**, pp. 192–196.

[2] Richtmyer, R., 1960. "Taylor instability in shock acceleration of compressible fluids". *Comm. Pure Appl. Math.,* **13**, pp. 297–319.

[3] Meshkov, E., 1969. "Instability of the interface of two gases accelerated by a shock wave". *Sov. Fluid Dyn.,* **4**, pp. 101–108.

[4] Brouillette, M., 2002. "The Richtmyer-Meshkov instability". *Annu. Rev. Fluid Mech.,* **34**, pp. 445–468.

[5] Zaitsev, S., Lazareva, E., Chernukha, V., and Belyaev, V., 1985. "Intensification of mixing at the interface between media of different densities upon the passage of a shock wave through it". *Sov. Phys. Dok.,* **30**(579).

[6] Brouillette, M., and Sturtevant, B., 1993. "Experiments on the Richtmyer-Meshkov instability: small-scale perturbations on a plane interface". *Phys. Fluids,* **5**(4), pp. 916–930.

[7] Houas, L., and Chemouni, I., 1996. "Experimental investigation of the Richtmyer-Meshkov instability in shock tube". *Phys. Fluids,* **8**, pp. 614–624.

[8] Poggi, F., Thorembey, M.-H., and Rodriguez, G., 1998. "Velocity measurements in turbulent gaseous mixtures induced by Richtmyer-Meshkov instability". *Phys. Fluids,* **10**, pp. 2698–2700.

[9] Leinov, E., Malamud, G., Elbaz, Y., Levin, L., Ben-Dor, G., Shvarts, D., and Sadot, O., 2009. "Experimental and numerical investigation of the Richtmyer-Meshkov instability under re-shock conditions". *J. Fluid Mech.,* **626**, pp. 449–475.

[10] Jones, M., and Jacobs, J., 1997. "A membraneless experiment for the study of Richtmyer-Meshkov instability of a shock-tube accelerated gas interface". *Phys. Fluids,* **9**, pp. 3078–3085.

[11] Weber, C., Haehn, N., Oakley, J., Rothamer, D., and Bonazza, R., 2012. "Turbulent mixing measurements in the Richtmyer-Meshkov instability". *Phys. Fluids,* **24**(074105).

[12] Erez, L., Sadot, O., Oron, D., Erez, G., Levin, L., Shvarts, D., and Ben-Dor, G., 2000. "Study of the membrane effect on turbulent mixing measurements in shock tubes". *Shock Waves,* **10**, pp. 241–251.

[13] Melling, A., 1997. "Tracer particles and seeding for particle image velocimetry". *Meas. Sci. Technol.,* **8**, pp. 1406–1416.

[14] Chauvin, A., Jourdan, G., Daniel, E., Houas, L., and Tosello, R., 2011. "Experimental investigation of the propagation of a planar shock wave through a two-phase gas-liquid medium". *Phys. Fluids,* **23**, p. 113301.

[15] Anderson, M., Puranik, B., Oakley, J., Brooks, P., and Bonazza, R., 2000. "Shock tube investigation of hydrodynamic issues related to inertial confinement fusion". *Shock Waves,* **10**, pp. 377–387.

[16] Wilson, B., Mejia-Alvarez, R., and Prestridge, K., 2013. "Simultaneous PIV and PLIF measurements of Mach number effects on single-interface Richtmyer-Meshkov mixing". 29th International Symposium on Shock Waves, Madison, Wi., July 14-19.

[17] Luo, X., Wang, X., and Si, T., 2013. "The Richtmyer-Meshkov instability of a three-dimensional air/SF6 interface with a minimum-surface feature". *J. Fluid Mech.,* **722**, p. R2.

[18] Jamme, S., Cazalbou, J.-B., Torres, F., and Chassaing, P., 2002. "Direct numerical simulation of the interaction of a shock wave and various types of isotropic turbulence". *Flow, Turbulence and Combustion,* **68**, pp. 227–268.

[19] Bouzgarrou, G., Bury, Y., Jamme, S., Joly, L., and Haas, J., 2013. "Experimental determination of the growth rate of Richtmyer-Meshkov induced turbulent mixing after reshock". 29th International Symposium on Shock Waves, Madison, Wi., July 14-19.

[20] Mohamed, M., and Larue, J., 1990. "The decay power law in grid-generated turbulence". *J. Fluid Mech.,* **219**, pp. 195–214.

List of Figures